Russian Chemical Reviews **80** (9) 855 – 868 (2011) © 2011 Russian Academy of Sciences and Turpion Ltd

DOI 10.1070/RC2011v080n09ABEH004184

Hydrogen in metallic nanomaterials

R A Andrievski

Contents

I.	Introduction	855
II.	The synthesis of nanocrystalline hydrides. Specific features of hydrogen absorption and desorption	855
III.	The absorption and desorption isotherms. Changes in the phase diagrams of metal – hydrogen systems	859
IV.	Properties of nanocrystalline metal hydrides	862
V.	Conclusion	865

Abstract. Problems concerning the synthesis of hydrogen-containing nanomaterials based on metals, alloys and intermetallics are considered. Characteristics of hydrogen absorption by and hydrogen desorption from these materials are analyzed. Specific features of the phase diagrams of metal – hydrogen systems in the case of nanostructured components are discussed. Data on the structure and defects, electronic structure and physicochemical properties of nanocrystalline metal hydrides are generalized; poorly studied problems in this field of research are outlined. The bibliography includes 99 references.

I. Introduction

The nanostructure approach has found increasing use in modern materials science. It utilizes the advantages of the nanostructure which is characterized by small sizes (from 1 – 2 to nearly 100 nm) of the key components (grains, inclusions, layers, pores, *etc.*). The possibility to obtain a vast variety of materials with unique physicochemical and physicomechanical properties attracts the attention of researchers and engineers. This manifests itself in both significant expansion of research and development and in a considerable increase in the amount of information in the field of nanochemistry (see, *e.g.*, Refs 1 and 2). Materials based on metal hydrides are promising for hydrogen-based power systems.[3 – 5] Nanostructuring of hydrides is of interest for significant activation of the synthesis conditions of nanomaterials and for control of their physicochemical properties.

Two reviews[6, 7] on the behaviour of hydrogen in nanostructures have been reported quite recently, but interest in nanostructured hydrides has increased considerably since then. This is indicated by publication of some reviews (see, *e.g.*, Refs 8 – 11), a monograph[12] and by the scope of the International Symposium 'Metal – Hydrogen Systems. Fundamentals and Applications' held recently at M V Lomonosov Moscow State University, Moscow, Russia.[13] Also, numerous interesting results were reported in original research articles and communications. The aforesaid gave the author an impetus to writing the present review.†

R A Andrievski Institute of Problems of Chemical Physics, Russian Academy of Sciences, prosp. Akad. Semenova 1, 142432 Chernogolovka, Moscow Region, Russian Federation. Fax (7-496) 522 35 07, tel. (7-499) 522 77 93, e-mail: ara@icp.ac.ru

Received 7 September 2010
Uspekhi Khimii **80** (9) 890 – 904 (2011); translated by A M Raevskiy

II. The synthesis of nanocrystalline hydrides. Specific features of hydrogen absorption and desorption

Main methods of synthesis of nanocrystalline hydrides include mechanochemical synthesis and hydrogenation of nanofilms and bulk nanostructured materials. The former method is most widely used. It involves high-energy milling of starting substances in inert media or in hydrogen. The foundations of mechanochemical synthesis were laid by Russian[14 – 16] and Canadian researchers.[17, 18] At present, the fundamental studies[14, 15] whose authors for the first time demonstrated the efficiency of mechanochemical synthesis for the preparation of magnesium alloys as materials for hydrogen power systems are cited rarely by Russian researchers and even less abroad. Extensive research in the field of mechanochemical synthesis has been carried out at the McGill University (Canada) and in other research centres.[12, 18]

Many researchers study magnesium alloys and compounds (magnesium hydride can store as many as 7.66 mass % of hydrogen). Our analysis will be focussed on the results obtained in studies of nanocrystalline magnesium compounds.

The kinetic curves for hydrogen sorption on magnesium powders with different particle size are shown in Fig. 1.[18] A

† The behaviour of hydrogen in carbon and organometallic nanostructures and in salt-like hydrides requires a separate comprehensive analysis and goes beyond the scope of this review.

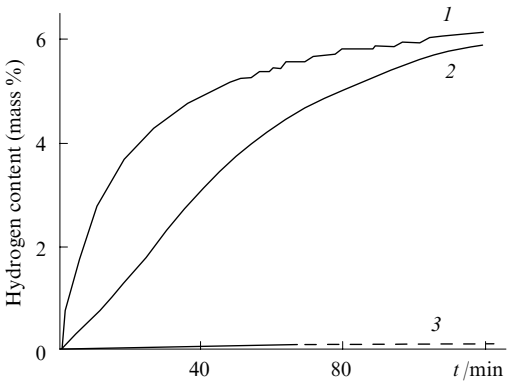


Figure 1. Kinetics of hydrogen sorption on magnesium powders with different particle sizes (T = 300 °C).[18]
Particle size: 30 nm (*1*), 50 nm (*2*) and 1 μm (*3*).

considerable advantage of the nanocrystalline particles obtained by high-energy milling is clearly seen. Reactive high-energy milling of magnesium powders in hydrogen atmosphere, as well as the use of catalytic additives (Pd, Ni, C, Mg_2Ni, Nb_2O_5, V_2O_5, *etc*.) and preparation of various nanocomposites ($MgH_2 + LiBH_4$, $CeCl_3 + NaAlH_4$, *etc*.) was also reported.[12, 13]

Milling is accompanied by a substantial decrease in the particle and grain size and by an increase in structural defectiveness of the particles (dislocations, packing errors, *etc*., appear). Finally, a hardly permeable surface oxide film is destroyed (it forms again on the surface of the milled particles). Attempts to differentiate the contributions of these factors to parameters of hydrogen desorption were made.[12, 19] Mention was made that milling of commercially available MgH_2 powders is accompanied by progressing formation of a high-temperature polymorph, *viz*., the γ-MgH_2 phase with high dissociation pressure.

The effect of the average size of magnesium hydride particles on the parameters of hydrogen desorption spectrum [initial desorption temperature, low- and high-temperature peaks (T_{LT} and T_{HT}, respectively)] is illustrated in Fig. 2.[19] In these experiments, the particle size was changed by varying the duration of milling in hydrogen (from 15 min to 100 h). Starting with 10-h milling, the X-ray diffraction patterns exhibited a progressing formation of the γ-MgH_2 phase. The data in Fig. 2 suggest a correlation between the desorption parameters of the particles whose size falls in a wide range from 400 to 36×10^3 nm and almost no correlation for nanocrystallites from 3 to 67 nm in size. The observed decrease in the initial desorption temperature (by about 60 °C), T_{LT} (by nearly 30 °C) and T_{HT} (by about 50 °C) were solely associated[12, 19] with the presence of the γ-phase; the role of crystallite size was thought to be insignificant.

The impact of the size effects was studied in detail taking the sorption properties of magnesium nanowires obtained by evaporation – precipitation in argon atmosphere (at 1203 and 503 K, respectively) as an example.[20] Nanowires 30 – 50 nm (batch 1), 80 – 100 nm (batch 2) and 150 – 170 nm in diameter (batch 3) were synthesized by varying the inert gas flow rate. The results of hydrogen absorption and desorption studies of these systems carried out at 373 – 573 K are shown in Fig. 3. As can be seen, the diameter of particles strongly affects the kinetics of hydrogen absorption and desorption. It is noteworthy that the effect changes as the temperature varies, as is particularly clearly seen when considering the mutual position of the kinetic curves at 573 K. Data processing showed that the activation energies of hydrogenation (E_{ah}) and dehydrogenation (E_{ad}) for batches 1, 2 and 3 are

Batch	1	2	3
E_{ah} /kJ (mole of H_2)$^{-1}$	33.5	38.7	70.3
E_{ad} /kJ (mole of H_2)$^{-1}$	38.8	46.5	81.1

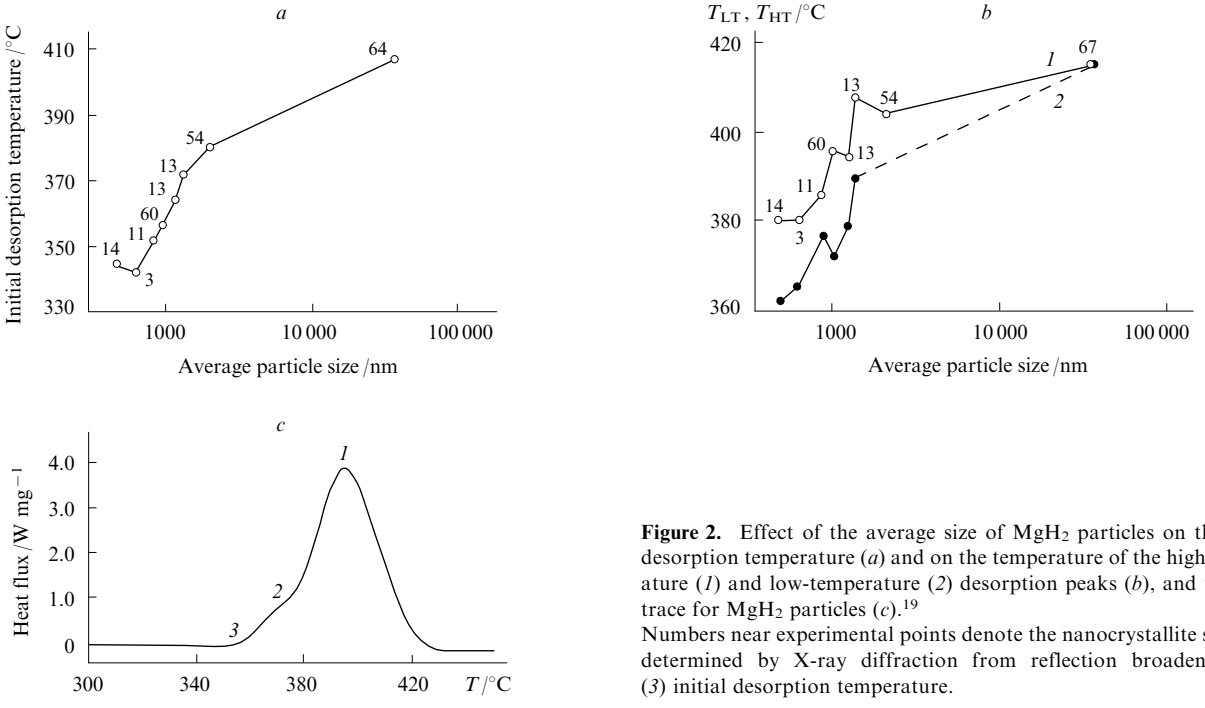


Figure 2. Effect of the average size of MgH_2 particles on the initial desorption temperature (*a*) and on the temperature of the high-temperature (*1*) and low-temperature (*2*) desorption peaks (*b*), and the DSC trace for MgH_2 particles (*c*).[19]
Numbers near experimental points denote the nanocrystallite size (nm) determined by X-ray diffraction from reflection broadening; (*c*): (*3*) initial desorption temperature.

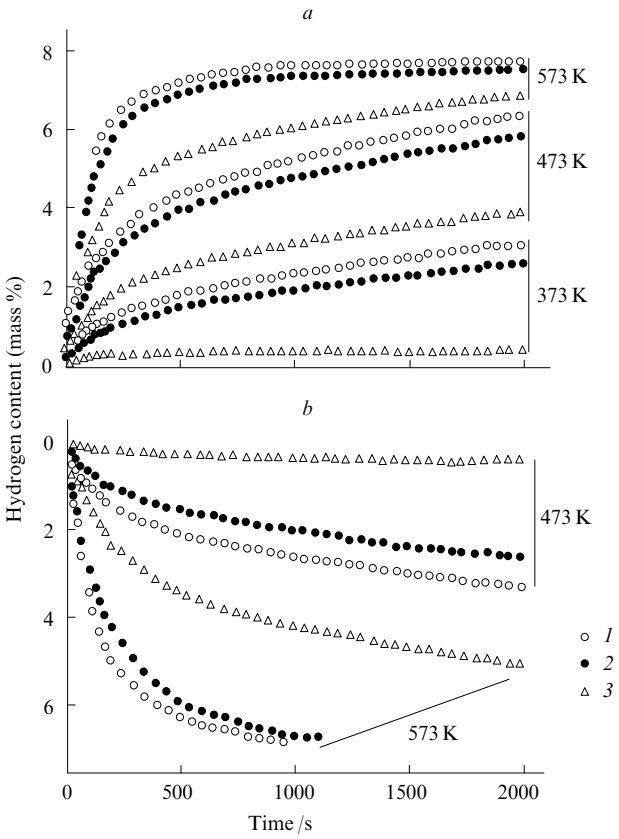


Figure 3. Kinetics of hydrogen absorption (*a*) and desorption (*b*) from magnesium nanowires of different diameter: 30–50 (*1*), 80–100 (*2*) and 150–170 nm (*3*).[20]

These values are much lower than the corresponding values for milled MgH_2 powders (120–142 kJ per mole of H_2). It was also found that nanowires from batch 1 break after ten hydrogenation–dehydrogenation cycles, although their composition did not change even after fifty cycles. For the hydride samples, only the traditional tetrahedral polymorph β-MgH_2 was observed, but, unfortunately, the size of nanocrystallites in nanowires was not reported in Ref. 20.

Recently, a number of studies on magnesium nanoparticles smaller than 5–10 nm in size were reported.[21–24] A nanocomposite MgH_2–0.5% TiH_2 was prepared by high-energy milling of starting hydrides in hydrogen under a pressure of 13.8 MPa for 4 h (ball-to-mixture mass ratio was 35 : 1).[21,22] According to X-ray diffraction data, the particle size was about 5 nm; transmission electron microscopy (TEM) and scanning electron microscopy (SEM) studies revealed a particle size interval from 5 to 10 nm.

Five-nanometre magnesium particles stabilized by tetrabutylammonium bromide were obtained by electrochemical synthesis.[23] Hydrogenation of these particles with hydrogen was carried out at a pressure of 2 MPa at 60 °C. Nanoparticles 2.8 ± 0.2 nm in size were obtained by colloidal synthesis and then saturated with hydrogen at a pressure of 3.3 MPa at 118 °C; the size of the hydride particles determined by X-ray diffraction is 5 nm.[24] After hydrogenation, the particles contained the β-MgH_2 phase (the titanium composites also contained the TiH_2 phase[21,22]); the amount of hydrogen was about 6.3 mass % (see Refs 21 and 22) and ~7.6 mass %.[23,24] Figure 4 presents the results of a hydrogen desorption study of magnesium hydride nanoparticles obtained by the methods used in Refs 21–24. These results and the data reported earlier[18,20] can be generalized as follows.

1. A positive effect of high-energy milling and of the decrease in the Mg and MgH_2 nanoparticle size on the parameters of hydrogen absorption and desorption is obvious and confirmed in many studies.

2. Small additives of TiH_2 nanoparticles favour acceleration of hydrogen absorption and desorption and a decrease in the initial desorption temperature (by about 100 °C from 280 to 180 °C). It is important that not only do

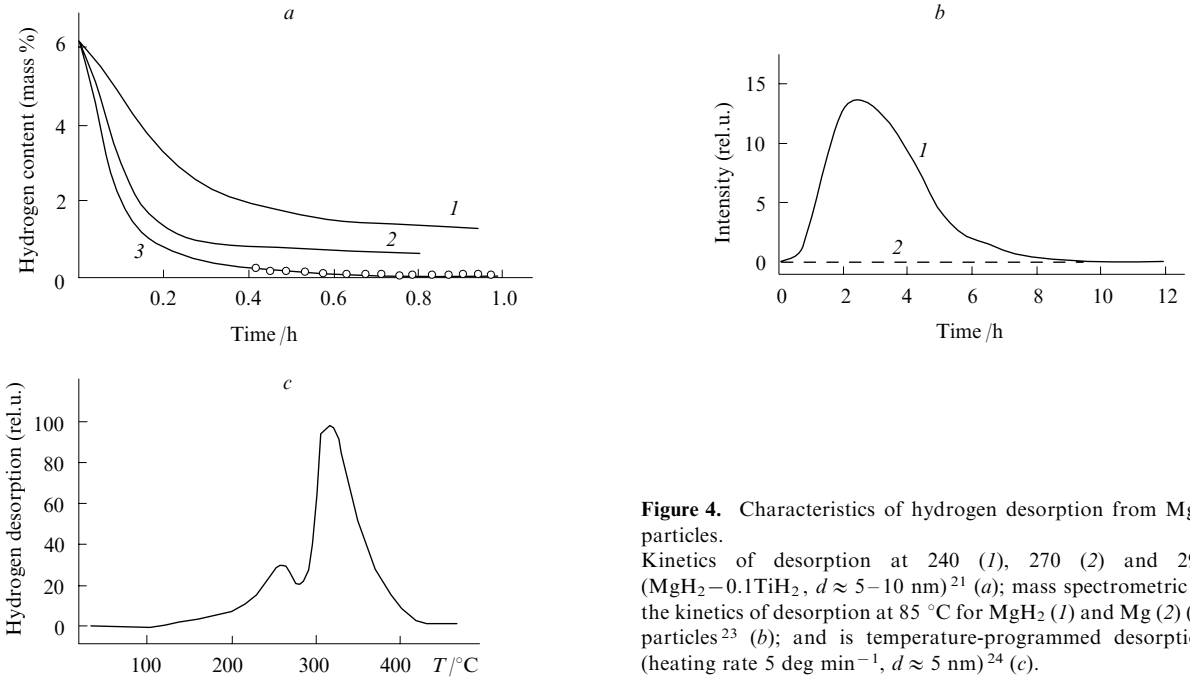


Figure 4. Characteristics of hydrogen desorption from MgH_2 nanoparticles.
Kinetics of desorption at 240 (*1*), 270 (*2*) and 290 °C (*3*) (MgH_2–$0.1TiH_2$, $d \approx 5$–10 nm)[21] (*a*); mass spectrometric picture of the kinetics of desorption at 85 °C for MgH_2 (*1*) and Mg (*2*) ($d \approx 5$ nm) particles[23] (*b*); and is temperature-programmed desorption profile (heating rate 5 deg min^{-1}, $d \approx 5$ nm)[24] (*c*).

these additives exhibit the catalytic effect, but also make the nanocomposite rather stable on multiple thermocycling (the composition of the samples remains almost unchanged after 80 hydrogenation–dehydrogenation cycles; this is much better than the results obtained for undoped MgH_2 nano- and microparticles). This was associated with the blocking effect of the additives on the growth of nanograins in the MgH_2 matrix.[21,22] An *in situ* TEM study of hydrogen desorption from $MgH_2 + Nb_2O_5$ composites showed that the formation of magnesium nanoparticles is observed at 150 °C.[25]

3. The possibility of hydrogen desorption from MgH_2 nanoparticles at 85 °C is remarkable. This is the lowest desorption temperature determined for nearly 5-nm nanoparticles (see Fig. 4*b*).[23] Hydrogen desorption is controlled by the nucleation and growth of seeds of the α-phase (a solid solution of hydrogen in magnesium) at the MgH_2/Mg interface; the diffusion kinetics is second in importance.

4. The initial desorption temperature for 5-nm MgH_2 nanoparticles decreases by 160–250 °C as compared with bulk magnesium hydride (see Fig. 4*c*). By and large, the data[24] differ from the results obtained in Ref. 23. Analysis of the reasons for these differences is difficult because many features of nanoparticles and synthesis conditions (*e.g.,* the structure of interfaces, the amounts of impurities and their segregations, residual strain, *etc.*) were not reported.

Hydrogenation–dehydrogenation processes are widely studied by SEM, TEM, micro electron diffraction analysis, energy-dispersive analysis and by electron energy loss spectroscopy (EELS). Figure 5 shows a micrograph of hydrogenated powders of $Mg_{85}Ni_{10}La_5$ alloy with a characteristic banded structure typical of such magnifications.[25] The phase composition was identified based on the interplanar spacings (l) and on EELS data. The hydride particles contained round, nearly 10-nm LaH_3 and Mg_2NiH_4 particles, both isolated or in the form of aggregated species (see Fig. 5) in the magnesium hydride matrix. The nanoinclusions retained their round shape after dehydrogenation at about 400 °C.

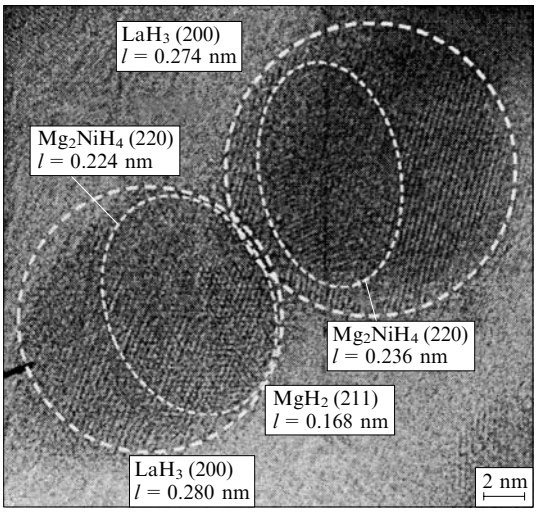


Figure 5. Micrograph of $Mg_{85}Ni_{10}La_5$ alloy powder after hydrogenation at 400 °C.[25]
Shown are the interplanar spacings (l).

Dehydrogenation of $MgH_2 + Nb_2O_5$ nanocomposite particles was studied *in situ* by high-resolution TEM in the temperature range from ambient temperature to 200 °C.[26] The catalytic effect of the additive (1 mass % Nb_2O_5) manifested itself at 150 °C where the formation of nearly 60-nm magnesium nanocrystals at the oxide/hydride interface was observed. For the composite $MgH_2 + 10$ mass % Nb_2O_5, decomposition of the hydride and the formation of MG nanocrystals at the interface were observed at room temperature; in this case, additional effects of electron irradiation in the electron microscope cannot be ruled out.

Phase transformations during hydrogenation–dehydrogenation of compounds based on Mg and the system Mg–Mm–Ni (Mm is the mischmetal) were studied by *in situ* high-resolution synchrotronous X-ray diffraction.[27] The initial samples were obtained by arc melting followed by plastic deformation and reactive ball milling in hydrogen atmosphere. The formation of two magnesium hydride polymorphs, β and γ, in a 7:3 ratio with a grain size of about 7 nm was observed. Thermal desorption at $T = 350$ °C was accompanied by the $\gamma \rightarrow \beta$ transition and growth of grains to nearly 20 nm; the magnesium crystallites formed were larger than 150 nm in size. Subsequent hydrogenation led to a decrease in the crystallite size to about 100 nm. Thus, the primary nanostructure is not conserved during hydrogenation–dehydrogenation cycling. By and large, the study[27] allowed one to reveal interesting features and the limiting stages of hydrogenation–dehydrogenation of magnesium and compounds in the system Mg–Mm–Ni.

Research on films is increasingly progressing in nanostructural materials science because these objects often allow one to exclude the influence of certain factors; this favours successive investigations on the role of the size effects.[6,7] The structure and properties of films based on metal hydrides were analyzed in reviews.[6,7,28] Hydrogen desorption from MgH_2 nanocrystalline thin films was also studied.[29] To prevent the films from oxidation, they were covered with hydrogen permeable thin palladium films (thickness ~10 nm). The results obtained for thick films (thickness 380 ± 20 nm, nanocrystallite size $\sim 80 \pm 20$ nm) and thin films (thickness 135 ± 15 nm, nanocrystallite size $\sim 30 \pm 10$ nm) are shown in Fig. 6. As can be seen, a complete desorption of hydrogen from thin films at room temperature in air takes about 2000 min while the thick films lose nearly 40% of the initial amount of hydrogen after this time. Evaluation showed that the diffusion coefficient of hydrogen in magnesium at room temperature is about 2×10^{-12} cm s^{-1}, being much lower than the published data. Taking account of this fact, it was concluded that hydrogen desorption from MgH_2 films is controlled by nucleation and growth of seeds at the MgH_2/Mg interface. This is in excellent agreement with the conclusions drawn in Ref. 23 (see above). Analysis of the thermodesorption spectra showed that the activation energy of desorption and the temperatures of peaks for the thick and thin films are almost equal (135 ± 20 kJ per mole of H_2 and ~148 °C); therefore, these parameters are independent of both film thickness and nanocrystallite size within the studied limits.

However, in spite of the representative information obtained in the experiments with nanowires[20] and films,[29] the impact of various factors on the size effects, as applied to the sorption properties of metal and metal hydride nanoparticles with a wide range of particle sizes (from ~100 to 1–2 nm), cannot be determined in 'pure' form.

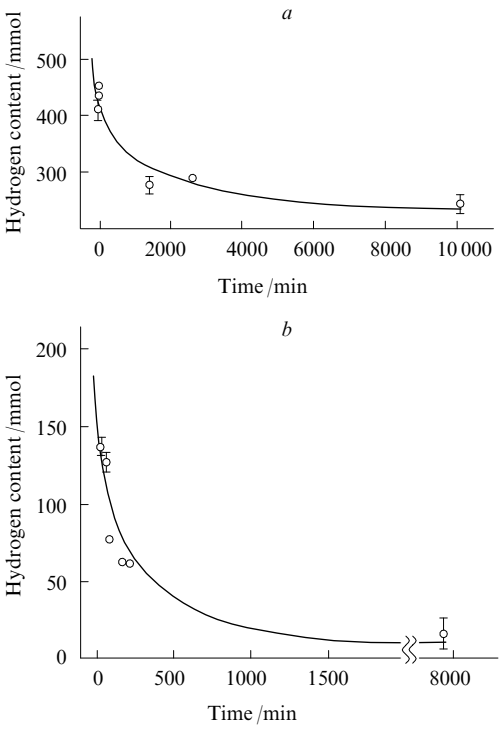


Figure 6. Kinetics of hydrogen desorption from thick (*a*) and thin (*b*) MgH_2 films at room temperature.[29]

The amount of information on hydrogenation of bulk nanomaterials obtained by intense plastic deformation (IPD) is smaller compared with the data arrays obtained for nanomaterials prepared by mechanochemical synthesis and for films (see above). Various IPD techniques [*e.g.*, high-pressure twisting (HPT), equal channel angular pressing, pack rolling, *etc.*] favour disintegration of microstructure and accumulation of deformation defects (see, *e.g.*, Ref. 30). A combination of equal channel angular pressing of a magnesium alloy ($\sim$5 mass % Zn and $\sim$0.7 mass % Zr) with high-energy milling causes the grain size to decrease to 20–30 nm. The process is accompanied by absorption of hydrogen (to 6.2 mass % at 300 °C), an increase in the dissociation pressure in the two-phase region, improvement of the kinetics of hydrogen desorption at 300 °C and by disappearance of hysteresis in the adsorption and desorption isotherms on hydrogenation–hydrogenation.[31]

Acceleration of hydrogen absorption by Mg–Ni and Mg–Mm–Ni eutectic alloys in the temperature range from 300 to 350 °C after equal channel angular pressing was reported.[32–34] Pack rolling studies aimed at obtaining multilayered samples (laminates) taking Mg/Ni and Mg/Cu layers as examples showed a promise of the method for improvement of the sorption properties (see, *e.g.*, Refs 6, 35, 36). A considerable decrease in the grain size (up to a few nanometres) was demonstrated in the case of palladium and palladium hydride when using HPT and extrusion–compression cycling.[37,38] Taking titanium as an example, it was shown that tensile strain significantly accelerates absorption of hydrogen, while compressive strain intensifies desorption of hydrogen; also, twins in the microstructure play some role.[39]

The HPT method was best studied using nanocrystalline magnesium samples as well as MgH_2 and $MgH_2 + 5\%$ Fe powders.[40] It was shown that even multiple HPT cycles at a pressure of 5 GPa do not lead to a decrease in the size of large crystalline grains to less than 2 μm. Only using pressed magnesium hydride powders pretreated under high-energy milling conditions, one can obtain small disk samples (7 mm in diameter and 0.3 mm in height) with crystallite sizes in the range 10–20 nm; the (101) texture was also reported. As in the case of milling,[19] the formation of γ-MgH_2 with the same crystallite size was detected by X-ray diffraction. Powder mixtures $MgH_2 + 5\%$ Fe behave analogously, but SEM studies revealed cracking in the compressed disks. A study of hydrogen sorption–desorption kinetics revealed a significant improvement of these properties at 300–350 °C. It was also reported that forging and rolling of conventional MgH_2 powders at room temperature produces samples with a crystallite size of 26 and 10 nm, respectively. However, the optimum IPD techniques are still unknown and the mechanism of the effect of induced defects on the sorption properties of bulk nanomaterials remains unclear.

Bulk nanomaterials also comprise nanoporous objects including nanoporous powders (pore size 2–3 nm) and the so-called metallic foams (see, *e.g.*, Ref. 41). Regularities of the behaviour of hydrogen in metallic foams based on palladium, iron, nickel, copper, silver, gold and other metals and alloys are important for the design of novel catalysts, devices for hydrogen storage and purification and for separation of hydrogen isotopes.

III. The absorption and desorption isotherms. Changes in the phase diagrams of metal–hydrogen systems

As applied to metals (M) in the nanocrystalline state, parameters of the hydrogen absorption and desorption isotherms have been best studied for palladium, a classical component of research on M–H_2 systems. Changes in the absorption isotherms on going from coarse-grained to nanocrystalline palladium at different temperatures are shown in Fig. 7. The transition is accompanied by an increase in the solubility of hydrogen in the α-phase of nanostructured palladium (H/Pd > 0.1–0.2), an increase in the partial pressure of hydrogen, a decrease in the concentration range of the palladium β-phase (H/Pd > 0.3) and narrowing of the two-phase region ($\alpha + \beta$).

The isotherms of hydrogen absorption and desorption by 5.2-nm and 3-nm palladium particles at room temperature are shown in Fig. 8. The changes in the hysteresis parameters due to the decrease in the critical decomposition temperature T_c [maximum temperature at which the two-phase region ($\alpha + \beta$) exists] are clearly seen. One can show, in the quasi-chemical approximation, that the observed decrease in T_c leads to a decrease in the mixing energy in the palladium–hydrogen system.[6,38]

Analogous results were obtained for nanostructured thin films of the hydrides Pd–H_2, Nb–H_2 and Ti–H_2.[27,43,44] Information on the phase boundaries in the system Ti–H_2 at room temperature for films (grain size 13–20 nm) and conventional coarse-grained samples is presented in Table 1.[43] As can be seen, broadening of the α-phase region and narrowing of the two-phase region ($\alpha + \beta$) is characteristic of nanostructured film samples. In

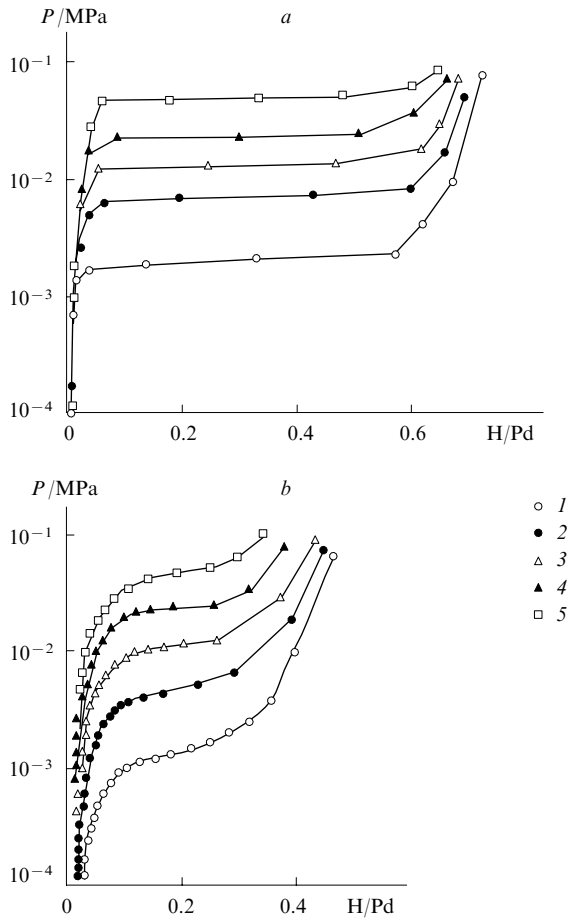


Figure 7. Isotherms of hydrogen absorption by coarse-grained (*a*) and nanocrystalline (*b*) (grain size ~10 nm) palladium at 298 (*1*), 323 (*2*), 338 (*3*), 353 (*4*) and 373 °C (*5*).[38]

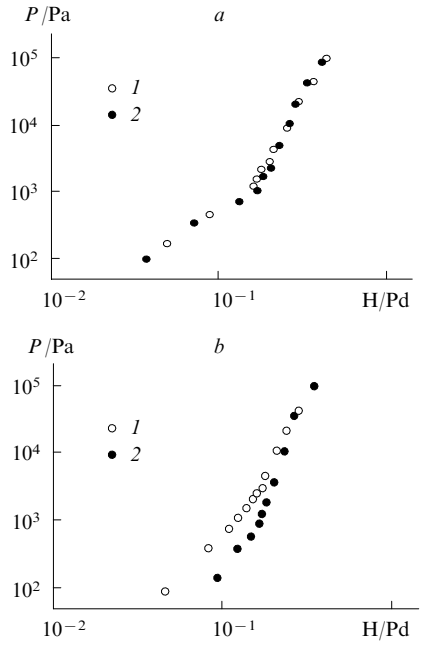


Figure 8. Isotherms of hydrogen absorption by (*1*) and desorption from (*2*) palladium particles at room temperature.[42]
Particle size 5.2 (*a*) and 3 nm (*b*).

Table 1. Characteristics of the α- and β-phases in the system $Ti-H_2$.[43]

Object	c_α (H/Ti)	c_β (H/Ti)
Film 100 nm thick on Al_2O_3 (0001) plane	0.1	0.7
Film 100 nm thick on Al_2O_3 (11$\bar{2}$0) plane	0.1	0.8
Film 220 nm thick on Al_2O_3 (0001) plane	0.1	0.4
Film 220 nm thick on Al_2O_3 (11$\bar{2}$0) plane	0.05	0.5
Coarse-grained samples	4×10^{-4}	1.5

Note. c_α and c_β are respectively the maximum and minimum hydrogen concentrations.

this case, a considerable compressive strain should be taken into account. The effect of the hydrogen concentration in films of different thickness on the residual compressive strain is illustrated in Fig. 9.[44] The residual strain determined by X-ray diffraction from the bending of films on substrates is larger for thin films (see Fig. 9), which are also characterized by greater changes in the phase diagram.

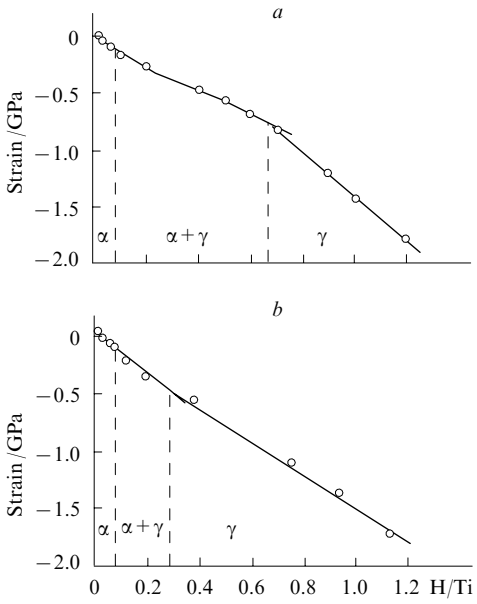


Figure 9. Residual compressive strain in $Ti-H_2$ films 220 (*a*) and 100 nm thick (*b*) plotted *vs*. hydrogen concentration.[44]
Dashed lines denote the existence regions of the phases α, (α + γ) and γ.

The results obtained in Refs 38 and 42 were confirmed and extended in the experiments with 2.5–7-nm palladium nanoparticles covered with polymeric films that do not absorb hydrogen[45] and placed in a mesoporous graphite matrix[46] (Table 2, Fig. 10). An *in situ* study of the phase composition allowed one to reveal specific features of dispersion in the intermediate stage of hydrogenation (see Fig. 10 *b*) from broadening of reflections on the X-ray diffraction patterns. These features appeared to be characteristic of both the metal and hydride.

If broadening of the α-region (increase in c_α) can be explained by additional 'dissolution' of hydrogen at nanograin boundaries and by the formation of hydride-like segregations on dislocations (see Ref. 47 and Section IV), the narrowing of the two-phase regions (α + β) and (α + δ) and a decrease in the concentration range of the β-phase (c_β)

Table 2. Characteristics of the α- and β-phases in the system Pd—H_2.[45]

Diameter /nm	c_α (H/Pd)	c_β (H/Pd)	$-\Delta H_{\alpha\to\beta}$	$-\Delta S_{\alpha\to\beta}$	T_c/K
Coarse-grained palladium					
—	0.03	0.55	∼36	∼90	565
Particle I					
7.0 ± 0.9	0.11	0.43	31 ± 1.8	67.3 ± 5.1	—
Particle II					
2.6 ± 0.4	0.12	0.38	34.6 ± 0.61	83 ± 1.8	393

Note. c_α and c_β is the maximum hydrogen concentration in the α- and β-phase, respectively (T = 303 K); $\Delta H_{\alpha\to\beta}$ [kJ (mole of H_2)$^{-1}$] and $\Delta S_{\alpha\to\beta}$ [J (mole of H_2)$^{-1}$ K^{-1}] are respectively the changes in the enthalpy of formation and in the entropy of the $\alpha\to\beta$ transition; T_c is the decomposition temperature.

are still to be clarified. Some assumptions concerning the subject were made. Based on analysis of the deformation changes in the palladium fcc cell induced by hydrogen insertion into the octahedral interstices, a hypothesis was proposed about hindrances to location of hydrogen at other positions and, correspondingly, about some changes in the hydrogen concentration.[38] At the same time, the deformation defects themselves can block the neighbouring positions for localization of hydrogen; this is accompanied by a decrease in configurational entropy and in the limited concentration of hydrogen in hydrides.[6] There are some indications of possible changes in the density of states and in the character of chemical bonds[45] as well as in the role of phase transitions.[46] In particular, mention was made that hydrogenation of 2.5-nm Pd nanoparticles causes a phase transition from the cuboctahedral to icosahedral structure and a decrease in the hydrogen content compared to its content in the coarse-grained β-phase.[46]

The size effect on the decomposition temperature of interstitial solid solutions was studied theoretically.[48] Taking into account the effect of elastic strain, it was shown

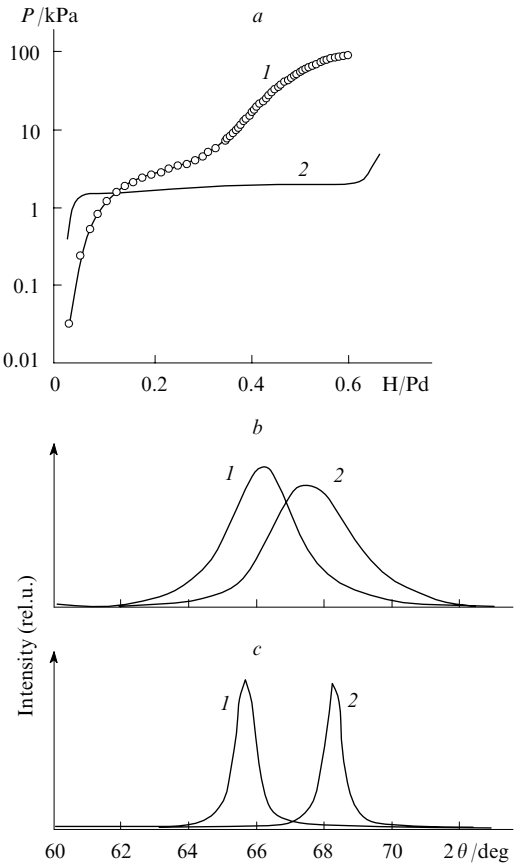


Figure 10. Isotherms of hydrogen absorption at 298 K (*a*) and the X-ray diffraction reflections (220) for coarse-grained palladium (*b*) and palladium nanoparticles (*c*).[46]
(*1*) hydride, (*2*) metal.

that a noticeable decrease in T_c begins if the particle size becomes equal to 20 nm and smaller. Experimental data[38] obtained for nearly 10-nm nanoparticles show a reasonable correlation with the results of calculations;[48] for nearly

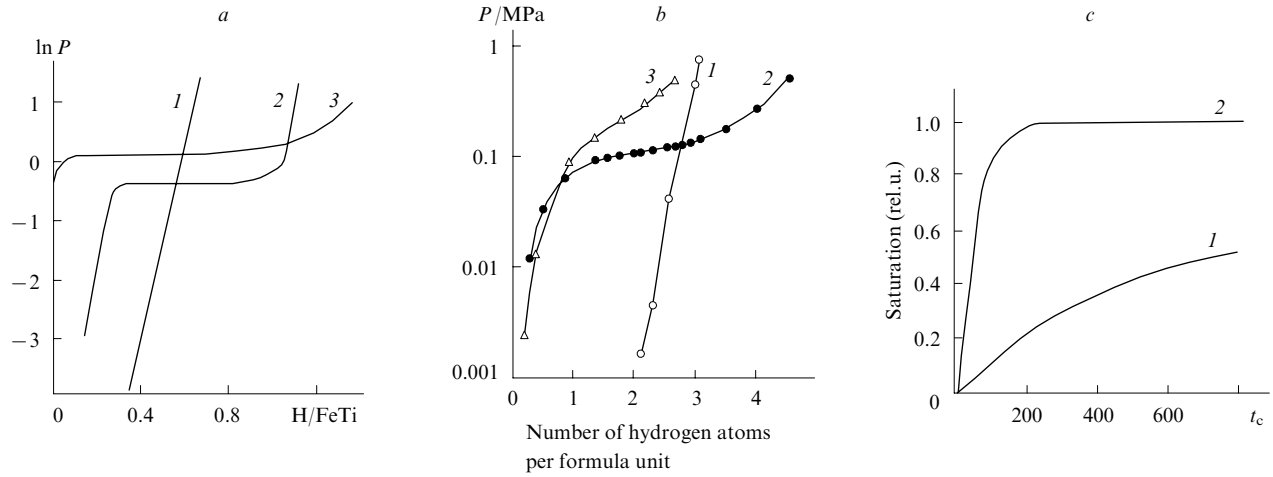


Figure 11. Isotherms of hydrogen absorption on intermetallics: FeTi at 293 K (*a*)[49] and $MmM_{5.2}$ at 328 K (*b*) and the kinetics of hydrogen absorption by the samples *1* and *2* (*c*).[50]
(*a*): Amorphous sample (*1*), nanocrystalline sample (grain size ∼6–7 nm) (*2*) and coarse-grained sample[49] (*3*);
(*b*): samples containing nearly 40% of amorphous phase (*1*), initial polycrystals (nanocrystallite size ∼54 nm) (*2*) and ∼15-nm nanocrystal (*3*),
(*c*): (*1*) and (*2*) are samples in (*b*).

2.5 nm nanoparticles, the experimental values are approximately twice as large as the calculated ones (see Table 2). The thermodynamic properties of the $\alpha \rightarrow \beta$ transition (see Table 2) calculated from the parameters of the absorption isotherms suggest some changes in the heat of formation and in the entropy with a decrease in the particle size. The parameters $\Delta H_{\alpha\rightarrow\beta}$ and $\Delta S_{\alpha\rightarrow\beta}$ of coarse-grained palladium change nonmonotonically; this was not explained so far.

Thus, the character of absorption isotherms suggests that the phase diagrams of metal–hydrogen systems prepared from nanosized components undergo the changes listed above. These changes become even more pronounced on going to amorphous objects, as was shown taking the systems $FeTi-H_2$ and $MmM_{5.2}-H_2$ as examples (Fig. 11).[49,50] In these experiments, nanocrystalline and amorphous samples were obtained by intense, high-energy ball milling. The phase analysis of the $MmM_{5.2}$ samples and the determination of crystallite sizes was based on X-ray diffraction profile analysis data. Figure 12 demonstrates a number of (111) reflections in the X-ray diffraction patterns of milled and annealed samples.[50] Data processing showed that the amount of amorphous phase after milling over a period of 3000 min was about 40% and the nanocrystallite size in the remaining crystalline phase was nearly 5 nm (see curve *2* in Fig. 12*a*). Additional annealing at 400 °C led to crystallization of the amorphous component with the formation of nanocrystalline phase (see curve *2* in Fig. 12*b*).

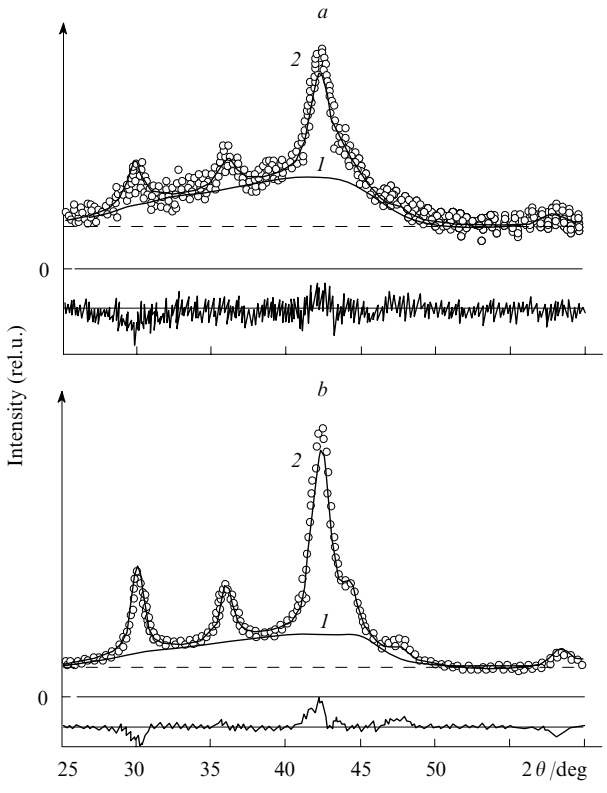


Figure 12. X-ray diffraction patterns of $MmM_{5.2}$ samples after milling over a period of 3000 min (*a*) and annealing at 175 °C (*b*).[50] Amorphous phase (*1*) and nanocrystalline phase (*2*) with a crystallite size of about 15 nm.

Within the limits of the studied hydride compositions, the phase diagrams of intermetallic–hydrogen systems show no two-phase regions for amorphous and amorphous-crystalline nanosized samples (see Fig. 11 *a*,*b*). A similar picture was also observed for the system $LaNi_5-H_2$ in a study of intermetallic powders after intense mechanical milling under different conditions.[51] Clearly, further detailed investigations of the nature and stability of phase equilibria in the nano scale (especially at particle sizes smaller than 3–5 nm) taking into account the transition from nanocrystalline to amorphous state are required. This will provide new information for assessment of the applicability of the notion 'phase' to nanosystems as well as new data on the structure of the phase diagrams of nonequilibrium systems comprising amorphous and nanocrystalline phases.

IV. Properties of nanocrystalline metal hydrides

1. Electronic structure

Main-group element hydrides are dielectrics with ionic and ionic-covalent bonds, whereas most transition-metal hydrides are metal-like compounds. Quantum chemical calculations of the electronic structure of hydrides allow one to elucidate the nature of chemical bonding in these systems and to compare their absorption capacities and stabilities. Such calculations are usually carried out within the framework of the density functional theory using the classical approximation (periodic boundary conditions) and the cluster approach (see, *e.g.*, Refs 52–55). For instance, it was shown [52] that the smaller the Mg and MgH_2 clusters the lower their stabilities, especially if the number of magnesium atoms is less than twenty. The hydrogen desorption energy significantly decreases if particles become smaller than 1.3 nm in size and the desorption temperature of 0.9-nm crystallites can be nearly 200 °C. As the cluster size decreases, the number of surface hydrogen atoms and hydrogen atoms in angular positions increases; correspondingly the total energy of M–H bonds decreases. The critical cluster size of simple (MgH_2 and CaH_2) and complex [$LiBH_4$, KBH_4, $Mg(AlH_4)$, *etc.*] hydrides is less than 2.5 nm with some variations depending on the shape of nanosystems (nanoparticles, nanowires, nanofilms, multilayered species) and on their polymorphs.[53]

Calculations of the clusters $Mg_{13}H_{26}$ and $Mg_{11}M_2H_{26}$ (M is the 3d-metal from scandium to zinc) [56] revealed changes in the Mg–Mg and Mg–H distances. It was concluded that doping of magnesium hydride with Sc, Ti, Cu and Zn atoms is promising for improvement of its thermodynamic properties. The results of calculations of the enthalpy of formation (see Fig. 13) are in qualitative agreement with the experimental data [11,57] (see also Fig. 4), although the possible catalytic effect (in the case of, *e.g.*, iron [40,58]) was left out of consideration.

A study of X-ray emission spectra demonstrated the formation of Ti–C, Ti–N and Ti–B bonds in titanium hydride after mechanochemical synthesis using titanium carbide, titanium nitride and boron nitride.[59] In addition, the BN and TiC additives have the strongest effect on the evolution of the titanium hydride spectra and on hydrogen desorption from this system.

As far as we know, such electronic characteristics as the electronic heat capacities, magnetic susceptibilities, Knight shifts and superconducting transition temperatures of nano-

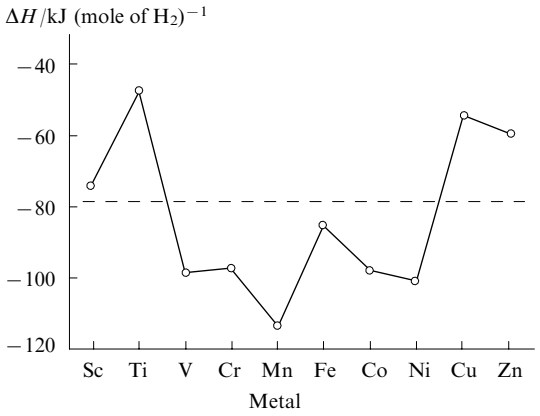


Figure 13. Changes in the enthalpy of formation of $Mg_{11}M_2H_{26}$ cluster for different 3d-metals.[56]
Horizontal dashed line corresponds to the calculated enthalpy of the cluster $Mg_{13}H_{26}$ [experimental value is nearly -75 kJ (mole of H_2)$^{-1}$].

crystalline 3d-metal hydrides [unlike niobium and nanocomposites based on copper (Cu – Nb and Cu – Pb)][60] were not reported so far. In any case, information on the subject is scarce and fragmentary.

2. The structure and defects

Peculiar features of the structure of nanocrystalline hydrides revealed by elastic and inelastic neutron scattering and the results of investigations of NMR spectra were reviewed;[6,7] therefore, in the text below we will only dwell on common regularities and on some unpublished data and new results, especially concerning structural defects.

Taking a nanostructured sample of iron – titanium deuteride $FeTiD_{0.97}$ (grain size about 10 nm) as an example, it was shown that nearly 50% of deuterium atoms are located at grain boundaries in tetrahedral positions near titanium atoms.[6] Inside grains, deuterium atoms occupy octahedral positions. The occupation of tetrahedral positions was also detected for nanocrystalline and amorphous iron – terbium deuteride samples. The NMR spectra of nanocrystalline $PdH_{0.72}$ clearly demonstrate peaks corresponding to internal hydrogen atoms and to the hydrogen atoms located at interfaces in a 1 : 2 ratio.[6]

The regularities of hydrogen dissolution in the α-phase of nanocrystalline palladium ($\leqslant$4.8 at.% H) were studied[61] by inelastic neutron scattering. Based on the intensities of the phonon spectra of the $PdH_{0.024}$ and $PdH_{0.048}$ nanoparticles nearly 15 nm in diameter and of a coarse-grained $PdH_{0.006}$ sample, hydrogen atoms in nanosized systems are mainly localized at interfaces, which leads to an increase in c_α (see Table 2). Both coarse-grained and nanocrystalline samples are characterized by almost equal hydrogen 'solubilities' in the α-phase grains. Thus, the assumption that hydrogen can occupy interstices in the nanostructure is incorrect.

Atom probe tomography was used to study the distribution of deuterium atoms in Fe/V multilayered films.[62,63] It was found that the deuterium concentration near interfaces decreases on going from the Fe/V interface towards the V/Fe interface. As the temperature decreased from 60 to 30 K, the initial inhomogeneous deuterium distribution became much more homogeneous. The need for further investigations to elucidate specific features of formation of alloys at interfaces was emphasized.[62,63]

Investigations of structural defects in nanocrystalline metal hydrides are concerned with a variety of effects of the size deformations appeared upon high-energy milling (mechanochemical synthesis), intense plastic deformation, formation of films, phase transformations, *etc*. In some cases (see, *e.g.*, Refs 64 – 66), deformation and other defects were studied by positron annihilation spectroscopy (PAS) which allows one to determine the presence of vacancies and their clusters (nanopores), as well as nanosegregations of particular alloy components. A PAS study of the defects that appear on milling of titanium and titanium hydride powders containing boron and hexagonal boron nitride additives in helium and $H_2 + He$ atmospheres showed[64] that the nanopore size and the probability of positron formation in these systems decrease with an increase in the milling time. Simultaneously, the titanium content in the vicinity of nanopores increases, which is associated with peculiarities of the behaviour of hydrogen and with the interaction of titanium with the additives in question. A smaller number of nanopores in the boron-containing samples was reported.

The behaviour of Mg and (Mg + Nb) films on hydrogenation and dehydrogenation was also studied by PAS.[65] The starting undoped magnesium films (grain size about 100 nm, total thickness 10 – 20 μm) prepared by high-frequency magnetron sputtering contained a large number of vacancies and vacancy clusters. After eight hydrogenation – dehydrogenation cycles, the doped films showed the formation of niobium clusters a few nanometres in size, which facilitated the desorption of hydrogen and the formation of magnesium seeds upon dehydrogenation.

Based on the properties determined by PAS, it was concluded that a vacancy in niobium irradiated with 10-MeV electrons and saturated with hydrogen is surrounded by one or two hydrogen atoms.[66] The concentration of such vacancy – hydrogen complexes is $(18-24)\times10^{-5}$ at.%. Further saturation of the samples with hydrogen leads to transformation of single-atom and diatomic hydrogen ensembles to quadrupoles surrounding niobium vacancies. These data indicate that PAS can be used as efficient tool for analysis of irradiated materials with low hydrogen content.

Vacancy – hydrogen complexes were also discovered in nanocrystals of the hydride $PdH_{0.78}$ (grain size 210 ± 60 nm) obtained by HPT (a version of the IPD technique) and investigated by SEM, TEM, densitometry and differential scanning calorimetry (DSC).[67,68] The concentration of thermal and deformation vacancies in coarse-grained palladium is usually at most 0.6 at.%; in the deformed hydride, it appeared to be considerably higher (1.3 at.% – 4.8 at.%), as was determined by densitometry, calorimetry and electron microscopy. This was associated with the formation of hydrogen complexes around the deformation vacancies. Taking into account the results of calorimetric measurements, it was assumed that the vacancy is surrounded by six hydrogen atoms. Hydrogen complexes can also form near other types of structural defects, *e.g.*, dislocations, intergrain boundaries, *etc*. A study involving thermal annealing of samples showed that a noticeable growth of nanograins begins at temperatures above 573 K. This gave grounds to consider these systems thermally stable.

3. Diffusion properties

It should be noted that the presence of a considerable amount of super-equilibrium vacancies in metal hydrides has long been debated regardless of nanomaterials (see, *e.g.*, Refs 69–71). It is accepted that hydrogen atoms favour an appreciable decrease in the energy of vacancy formation; as a consequence, the concentration of vacancies increases, which significantly affects the processes of self- and hetero-diffusion. In particular, the self-diffusion coefficient of ^{95}Nb in the niobium hydrides $NbH_{0.05}$ and $NbH_{0.34}$ increases with an increase in the hydrogen concentration while the activation energy of diffusion decreases.[70] Thus, the results of studies [66–68] contribute to progress in research on metal hydrides [71] and give an impetus to further investigations of diffusion and diffusion-controlled processes.

Information on such processes in nanocrystalline metal hydrides is restricted to the studies of corresponding NMR spectra. The activation energies of self-diffusion of hydrogen in nanocrystalline vanadium hydride are listed in Table 3.

Considerable attention was paid to the preparation and certification of the systems under study.[72] Samples were prepared under controlled milling and saturation with hydrogen. Particles of the hydride powder were 1–10 μm in size and the crystallite sizes were 10–80 nm (according to X-ray diffraction data) depending on the milling duration. Without dwelling on specific features of the methods for separation of the effects of total, bulk and grain boundary diffusion, mention may be made that the data of Table 3 clearly indicate the effect of the crystallite size on the activation energy (especially for the temperature range 200–300 K) in spite of some difference in the compositions. Some difference in the character of this effect for the temperature intervals 120–200 and 200–300 K is due to the phase transformations occurring in these temperature and composition ranges, which manifests itself in a complex phase diagram of the $V-H_2$ system (see Fig. 1 in Ref. 72). Based on the estimate of the frequency factor in the diffusion equation, it was concluded that the diffusion mobility of hydrogen in the near-boundary regions is much higher than inside crystallites. Mention was made [72] that it is unclear why the value $Q_v = 120$ meV (see Table 3) differs from the activation energy of total diffusion of coarse-grained hydride $VH_{0.62}$ equal to 240 meV. The obtained values Q, Q_v and Q_g, as well as their dependences on the crystallite size are still to be clarified.

The effect of the duration of milling of the hydrides $ZrCr_2H_3$, MgH_2 (doped with V_2O_5 and Al) and TiH_2 (doped with C, B and BN) on the NMR spectra was studied.[73,74] According to X-ray diffraction data, the crystallite sizes in the experiments varied from 10 to 60 nm. For the zirconium chromium hydride it was found that an increase in the milling time leads to appreciable decrease in the mobility of hydrogen atoms owing to an increase in the proportion of disordered intercrystallite regions and amorphous component. Contrary to this, an increase in the milling time of magnesium hydride led to a significant increase in the NMR spectral parameters characterizing the mobility of hydrogen, but the 'provocative' role of paramagnetic centres formed in the course of milling was also reported. The ^1H and ^{11}B NMR spectra of titanium hydride were studied in the temperature interval 11–384 K. The mobility of hydrogen atoms in the nanocomposites TiH_2-BN was found to be higher than in TiH_2-C and TiH_2-B due to loosening of the TiH_2 lattice under nitrogen diffusion conditions. Two characteristic jumps of the hydrogen atom were also revealed.

It is quite obvious that parameters of hydrogen diffusion in the nanohydrides should be refined taking into account not only the boundary and bulk mass transfer, but also the presence of dislocation-type defects, twins, triple junctions and amorphous inclusions (see, *e.g.*, Ref. 75), as well as oxide films. This information is of fundamental importance for understanding of hydrogenation–dehydrogenation and for carrying out relevant calculations.

4. Physical properties

To date, the electrical properties of hydride nanofilms have been best studied.[6] The results of investigations of the electrical resistance of hydride films are often used to disclose the role of different factors in the formation of charge transfer properties and to estimate the hydrogenation–dehydrogenation parameters. The electrical resistance of thin films is governed by the scattering of charge carriers by phonons, grain boundaries, impurities and segregations, structural defects, the surface of films and by rough surface regions.[75] Also, one should take into account internal residual strain in the film and the curvature of its surface. The effect of nanostructure and residual strain were best studied for palladium films 30–200 nm thick (crystallite size 15–22 nm) supported on various substrates [nanocrystalline silicon (100), sapphire (0001), potassium bromide] and saturated with hydrogen at a pressure of 10^5 Pa and under electrochemical treatment conditions.[76] As a result, the effect of the composition on the properties of such films was refined. In particular, it was shown that an increase in the electrical resistance of the PdH_x films upon hydrogenation to $x = 0.2$ (region on the left of the vertical line in Fig. 14) is independent of film thickness. A feasibility analysis of the known Sieverts law relating the hydrogen concentration to its pressure at saturation showed that the Sieverts constant for the films is much larger than that of coarse-grained samples and increases upon re-hydrogenation. It was concluded that the effect of mechanical strain

Table 3. Activation energies (meV) of hydrogen self-diffusion in vanadium hydride crystallites of different size.[72]

Composition	Grain size /nm	Q		Q_v	Q_g	
		120–200 K	200–300 K	200–300 K	120–200 K	200–300 K
$VH_{0.82}$	80	41 ± 11	155 ± 3	172	–	180 ± 12
$VH_{0.73}$	30	48 ± 3	121 ± 4	120	59 ± 9	134 ± 4
$VH_{0.67}$	10	67 ± 5	80 ± 2	–	67 ± 5	80 ± 2

Note. Q is the activation energy of diffusion, Q_v is the activation energy of bulk diffusion, Q_g is the activation energy of grain boundary diffusion.

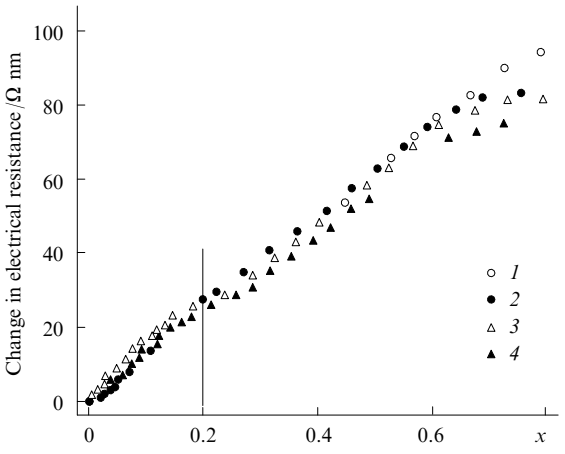


Figure 14. The increase in the electrical resistance upon hydrogenation of palladium films on sapphire substrate plotted *vs.* hydrogen content.[76]
Film thickness /nm: 35 (*1*), 74 (*2*), 144 (*3*) and 230 (*4*).

on the thermodynamic properties of thin films dominates the structural effects.

The behaviour of $Mg_{95-85}Cu_{0.5-15}$ films in hydrogenation–dehydrogenation was studied by monitoring the electrical resistance.[77] The role of nanocrystallinity (crystallite sizes 30–50 nm) and amorphism of the initial films was determined as the substrate temperature decreases from 298 to 223 K. Changes in the normalized increase in the electrical resistance of films in isochronous sorption experiments are shown in Fig. 15.[77] As the hydrogenation temperature decreased, the film $Mg_{95}Cu_{0.5}$ retained the nanocrystalline structure and its electrical resistance changed only slightly (Fig. 15 *a*). The films with higher copper content underwent amorphization, which manifested itself in a four- or fivefold increase in the electrical resistance. Also, it follows that amorphous films $Mg_{90}Cu_{10}$ and $Mg_{85}Cu_{15}$ are characterized by rather low desorption temperatures. The amorphous film $Mg_{90}Cu_{10}$ with a hydrogen content of 5.9 mass % and a desorption temperature of about 100 °C is recommended for practical applications.

Unfortunately, yet another important property of transfer phenomena, *viz.*, thermal conductivity of nanocrystalline hydrides has almost not been studied.

The optical properties of Mg_yNiH_x ($2 \leqslant y \leqslant 10$) films were studied and their dielectric properties were assessed.[78] A comparison of experimental data with the results of calculations of various mixtures $MgH_2 + MgNiH_4$ (a dielectric and a semiconductor with a forbidden gap of 5.6 and 1.6 eV, respectively) showed a reasonable correlation between experimental and calculated data for the compositions with low magnesium content ($y \leqslant 3.5$).

The evolution of magnetic states of chromium atoms in Cr/V multilayered films (layer thickness 50 and 1.4 nm) during saturation with hydrogen was studied.[79] It was shown that hydrogen uptake by individual Cr layers increases the sensitivity of detection of magnetic parameters including the Néel temperature.

Hydrogen 'dissolved' in nearly 15-nm ZnO nanoparticles (ZnO is a wide-gap semiconductor) causes a two- or threefold increase in the concentration of electrons, a considerable (by a few orders of magnitude) increase in conductivity and enhancement of IR reflectance.[80]

V. Conclusion

As mentioned above, additional investigations of poorly studied problems in the synthesis of hydrogen-containing nanomaterials based on metals, alloys and intermetallics are required. The role of the electronic structure, chemical composition and other characteristics of metal hydride nanoparticles should also be clarified. For instance, attritor grinding and cryomilling of $ZrAl_2$ intermetallic particles to a particle size of 10–20 nm followed by saturation with hydrogen at pressures of 2–6 MPa ($T = 150$ °C) was almost not accompanied by hydrogenation.[81] Replacement

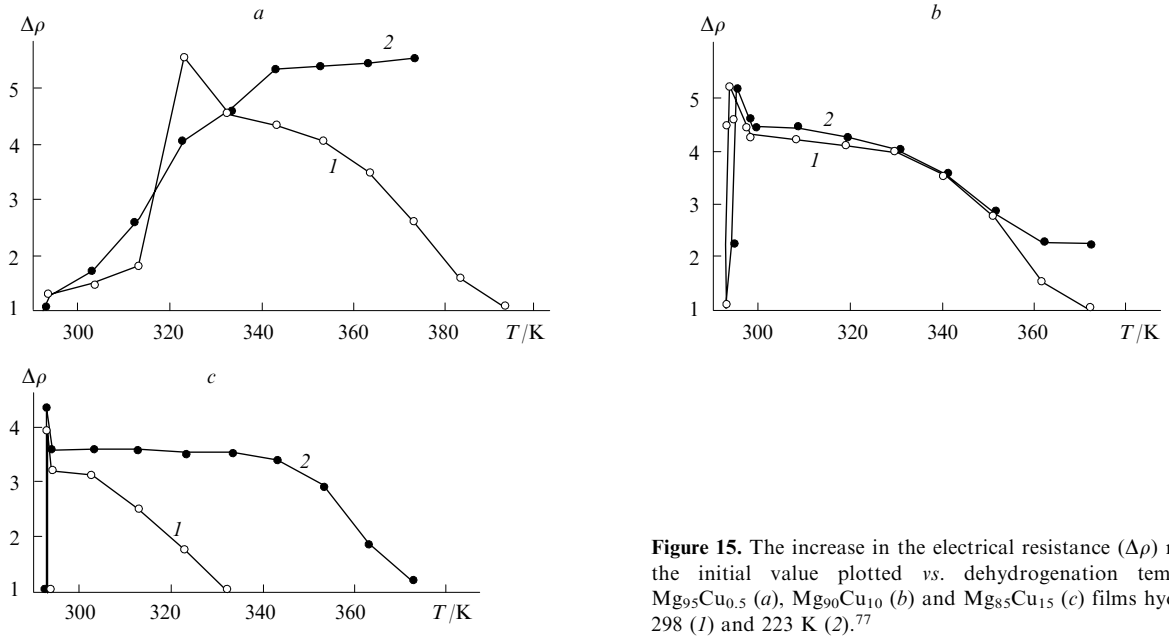


Figure 15. The increase in the electrical resistance ($\Delta\rho$) normalized to the initial value plotted *vs.* dehydrogenation temperature for $Mg_{95}Cu_{0.5}$ (*a*), $Mg_{90}Cu_{10}$ (*b*) and $Mg_{85}Cu_{15}$ (*c*) films hydrogenated at 298 (*1*) and 223 K (*2*).[77]

of 50% of Al atoms by Co atoms led to formation of the monohydride phase, but the hydrogen content in this phase was 20% lower than in the coarse-grained samples. It was concluded [81] that nanostructuring only leads to changes in the kinetic parameters of sorption and desorption, leaving the key thermodynamic properties unaffected. In this connection, detailed studies of the role of the size-dependent effects in the formation of the nanohydride properties still seem to be topical.[6, 7, 82] Compared to other compounds and metals,[60] nanohydrides have been less studied. In this review, we mainly analyzed the hydrogen-containing nanomaterials based on magnesium, palladium and titanium for which information is available. Analogous studies of hydrides based on intermetallics and other transition and main-group metals are to be carried out.

The need to compare the sorption and desorption parameters for different methods of synthesis of nanohydrides should be emphasized. This is necessary to disclose the role of 'technological trail', *i.e.*, the effect of the residual strain and the states of interfaces, the tendency to segregation of impurities, the rate of heating and cooling, *etc.*

Also, the phase diagrams of the M–H_2 systems should be studied and calculated in the framework of the $P-c-T$-approximation, as was demonstrated [83] for many binary systems under variable gas (oxygen, nitrogen, *etc.*) pressure conditions. In addition, hydrogen as dopant in nanosized metal samples (see, *e.g.*, Refs 84–86) induces superplasticity in zirconium, milling of structure in Cu–Ti alloys, a less brittle behaviour of nanocrystalline titanium, *etc.*

Considering prospects for the use of nanosized metal hydrides, one should also take into account the progress in the development of hydrogen-containing carbon and organometallic nanostructures, zeolites and multimolecular objects as well as complex hydrides (see, *e.g.*, Refs 87–89). Nanocrystalline metal hydrides, alloys and intermetallics are promising for the design of devices for hydrogen storage in transport, power sources, sensorics, *etc.*,[12] owing to reversibility of hydrogenation–dehydrogenation reactions, a wide range of operating pressures and temperatures, reasonable kinetic parameters and characteristics of stationary and mobile hydrogen storage. The nanostructure approach in the design of novel hydride materials is particularly appropriate in the case of magnesium and magnesium alloys (see above and Refs 11, 12, 57)

Small-scale experimental magnesium hydride tanks 270 cm^3 in volume with an effective capacity of 5.8 mass % H_2 were designed and tested in France.[90] One tank was filled with 123 g of milled MgH_2 and 4% of Ti–V–Cr alloy additive, while the other represented a 156-g pellet made of a mixture $MgH_2 + 5\%$ C (expanded natural graphite). The graphite additive made it possible to improve the thermal conductivity of the system and to significantly reduce the duration of the hydrogenation–dehydrogenation cycle (25 min at $P = 1.1$ MPa and $T = 300$ °C *vs.* nearly 3 h at $P = 0.1$ MPa and $T = 330$ °C). Researchers at McPhy Energy S.A. (France) struggle to design commercially available production.

Other applications in which the analyzed features of the behaviour of hydrogen in metallic nanomaterials can be useful include, *e.g.*, the following:

— use of palladium nanoparticles stabilized by films of biologically active molecules in catalysis and sensor techniques;[91] application of palladium nanofilms in electrochromic mirrors [92] and in highly sensitive hydrogen sensors;[76, 93]

— application of hydrogen-containing nanomaterials in nickel hydride power sources;[87, 94]

— various applications of nanocrystalline zinc oxide in electronics and optoelectronics can be extended owing to dissolution of hydrogen, which should significantly improve the electrical and optical properties;[80]

— dissolution of hydrogen in Cr/V-type multilayered nanostructures can significantly enhance the potential of magnetoresistive sensors.[79]

An analysis made in this review also seems to be useful for consideration of erosion phenomena in ITER plasma where hydrogen isotopes interact with nanofilms and nanoparticles under neutron irradiation conditions.[95]

In addition to a promising combination of the high-energy milling and HPT techniques,[40] noteworthy is multiple rolling of commercially available MgH_2 powders [96] and polymer–hydride nanocomposites [5-nm Mg nanoparticles in poly(methyl methacrylate) matrix] with a hydrogen content of about 6 mass.% (calculated with respect to the mass of Mg, *i.e.*, nearly 79% of the theoretical capacity of MgH_2) and admissible kinetic parameters.[97]

Summing up, intensive research and development of nanomaterials based on MgH_2 is followed by investigations on AlH_3 containing 10.1 mass % of H_2; studies on the synthesis of this system are increasingly progressing.[98, 99]

The author expresses his gratitude to many colleagues who kindly provided with their studies and presentations submitted to the International Symposium 'Metal–Hydrogen Systems. Fundamentals and Applications' held at M V Lomonosov Moscow State University, Moscow, Russian Federation, on July 19–23, 2010, and cited in this review.

This review has been written with the financial support from the Russian Foundation for Basic Research (Project No. 06-03-07009) and the Presidium of the Russian Academy of Sciences (Basic Research Programme, Subprogramme P-22).

References

1. Yu D Tretyakov, E A Gudilin *Russ. Chem. Rev.* **78** 801 (2009); *Usp. Khim.* **78** 867 (2009)
2. I V Zibareva, A V Zibarev, V M Buznik *Khim. Interes. Ustoichiv. Razv.* **18** 215 (2010) [a]
3. B P Tarasov, M V Lototskii, V A Yartys' *Ros. Khim. Zh.* **50** (6) 34 (2006) [b]
4. V N Verbetskii, S V Mitrokhin *Materialovedenie* (1) 48 (2009)
5. *Trudy III Mezhdunarodnogo Simpoziuma po Vodorodnoi Energetike* (Proceedings of IIIrd International Symposium on Hydrogen Power Engineering) (Moscow: (Moscow: Moscow Engineering Institute, 2009)
6. R A Andrievski *Usp. Fiz. Nauk* **177** 721 (2007) [c]
7. R A Andrievski *Mater. Sci. Forum* **555** 327 (2007)
8. M Niemann, S Srinivasan, A Phani, A Kumar, D Goswani, E Stefanakos *J. Nanomater.* **3** 1 (2008)
9. M Fichtner *Nanotechnology* **20** 204009 (2009)
10. S Sepehri, G Cao, in *Annual Review of Nano Research* Vol. 3 (Eds G Cao, Q Zhang, C J Brinner) (New York: World Scientific Publ., 2019) p. 487
11. L P Jain, Ch Lal, A Jain *Int. J. Hydrogen Energy* **35** 5133 (2010)
12. R A Varin, T Czujko, Z S Wronski *Nanomaterials for Solid State Hydrogen Storage* (New York: Springer, 2009)

13. *International Symposium 'Metal – Hydrogen Systems. Fundamentals and Applications' (Book of Abstracts)* Pts I, II (Moscow: Moscow State University, 2010)
14. I G Konstanchuk, E Yu Ivanov, V V Boldyrev *Dokl. Akad. Nauk SSSR* **286** 385 (1986) [d]
15. E Ivanov, I Konstanchuk, A Stepanov, V Boldyrev *J. Less-Common Met.* **131** 25 (1987)
16. I G Konstanchuk, E Yu Ivanov, V V Boldyrev *Russ. Chem. Rev.* **67** 69 (1998); *Usp. Khim.* **67** 75 (1998)
17. L Zaluski, A Zaluska, J O Ström-Olsen *J. Alloys Compd.* **217** 245 (1995)
18. A Zaluska, L Zaluski, J O Ström-Olsen *Appl. Phys. A* **72** 157 (2001)
19. R A Varin, T Czujko, Z Wronski *Nanotechnology* **17** 3856 (2006)
20. W Li, Ch Li, H Ma, J Chen *J. Am. Chem. Soc.* **129** 6710 (2007)
21. J Lu, Y J Coi, Z Z Fang, H Y Sohn, E Rönnebro *J. Am. Chem. Soc.* **131** 15843 (2009)
22. J Lu, Y J Coi, Z Z Fang, H Y Sohn, E Rönnebro *J. Am. Chem. Soc.* **132** 6616 (2010)
23. K-F Aguey-Zinsou, J-R Ares-Fernandez *Chem. Mater.* **20** 376 (2008)
24. S B Kalidindi, B R Jagirdar *Inorg. Chem.* **48** 4524 (2009)
25. K Tanaka, T Miwa, K Sasaki, K Kuroda *J. Alloys Compd.* **478** 308 (2009)
26. Sh Isobe, A Ono, H Yao, Y Wang, N Hashimoto, S Ohnuki *Appl. Phys. Lett.* **96** 223109 (2010)
27. R V Denys, A B Riabov, J O Maehlen, M V Lototsky, J K Solberg, V A Yartys *Acta Mater.* **57** 3989 (2009)
28. A Pundt, R Kirchheim *Annu. Rev. Mater. Res.* **36** 555 (2006)
29. J R Ares, F Leardini, P Diaz-Chao, J Bodega, D W Koon, I J Ferrer, J F Fernández, C Sánchez *J. Alloys Compd.* **405** 650 (2010)
30. R Z Valiev, I V Aleksandrov *Ob"emnye Nanostrukturnye Metallicheskie Materialy: Poluchenie, Struktura i Svoistva* (Bulk Nanostructural Metal Materials: Production, Structure and Properties) (Moscow: Akademkniga, 2007)
31. V M Skripnyuk, E Rabkin, Y Estrin, R Lapovok *Acta Mater.* **52** 405 (2004)
32. V Skripnyuk, E Buchman, E Rabkin, Y Estrin, M Popov, S Jorgesen *J. Alloys Compd.* **436** 99 (2007)
33. S Løken, J K Solberg, J P Maehlen, R V Denys, M V Lototsky, B P Tarasov, V A Yartys *J. Alloys Compd.* **446 – 447** 114 (2007)
34. P M Fursikov, in *Trudy III Mezhdunarodnogo Simpoziuma po Vodorodnoi Energetike* (Proceedings of IIIrd International Symposium on Hydrogen Power Engineering) (Moscow: Moscow Engineering Institute, 2009) p. 192
35. T T Ueda, M Tsukahara, Y Kamiya, Sh Kikuchi *J. Alloys Compd.* **386** 253 (2005)
36. K Tanaka, T Kiyobayashi, N Takeichi, H Miyamura, Sh Kikuchi *Mater. Sci. Forum* **638 – 642** 1143 (2010)
37. V A Teplov, V P Pilyugin, V S Gaviko, V Shchegoleva, I V Gervas'eva, A M Patselov *Fiz. Met. Metalloved.* **84** 525 (1997)
38. T Kuji, Y Matsumera, H Uchida, T Aizawa *J. Alloys Compd.* **330 – 332** 718 (2002)
39. H Suzuki, H Tanigychi, N Hanada, K Takai, Y Hagihara, in *International Symposium 'Metal – Hydrogen Systems. Fundamentals and Applications' (Book of Abstracts)* Pt. II (Moscow: Moscow State University, 2010) p. 301
40. D R Leiva, A M Jarge, T T Ishikawa, J Huot, D Fruchart, S Miraglia, C S Kiminami, W J Botta *Adv. Eng. Mater.* **12** 786 (2010)
41. B C Tappan, S A Steiner III, E P Luther *Angew. Chem. Int. Ed.* **49** 4544 (2010)
42. A Pundt, M Suleiman, C Bähtz, M T Reetz, R Kirchheim, N M Jisrawi *Mater. Sci. Eng., B* **108** 19 (2004)
43. E Tal-Gutelmacher, R Gemma, A Pundt, R Kirchheim *Acta Mater.* **58** 3042 (2010)
44. E Tal-Gutelmacher, A Pundt, R Kirchheim *J. Mater. Sci.* **45** 6389 (2010)
45. M Yamauchi, R Ikeda, H Kitagawa, M Takata *J. Phys. Chem. C* **112** 3294 (2008)
46. C Zlotea, F Cuevas, V Paul-Boncour, E Leroy, Ph Dibando, R Gadiou, C Vix-Guteri, M Latroche *J. Am. Chem. Soc.* **132** 7720 (2010)
47. Yu S Nechaev *Usp. Fiz. Nauk* **171** 1251 (2001) [c]
48. J Weissmüller, Ch Lemier *Philos. Mag. Lett.* **80** 411 (2000)
49. L Zaluski, A Zaluska, P Tessier, J O Ström-Olsen, R Schulz *J. Mater. Sci.* **31** 695 (1996)
50. J Ares, F Cuevas, A Percheron-Guegan *Acta Mater.* **53** 2157 (2005)
51. R A Andrievski, B P Tarasov, I I Korobov, N G Mozgina, S P Shilkin *Int. J. Hydrogen Energy* **21** 949 (1996)
52. R W P Wagemans, J H van Lenthe, P E de Jongh, A J van Dillen, K P de Jong *J. Am. Chem. Soc.* **127** 16675 (2005)
53. P Vajeeston, P Ravindran, H Hjellväg, in *International Symposium 'Metal – Hydrogen Systems. Fundamentals and Applications' (Book of Abstracts)* Pt. I (Moscow: Moscow State University, 2010) p. 29
54. M Yu Siretskiy, M G Shelyapina, D Fruchart, S Miraglia, N E Skryabina *J. Alloys Compd.* **480** 114 (2009)
55. M G Shelyapina, D Fruchart, P Wolfers *Int. J. Hydrogen Energy* **35** 2025 (2010)
56. M G Shelyapina, M Yu Siretskii *Fiz. Tv. Tela* **52** 1855 (2010) [e]
57. K-F Aguey-Zinsou, J-R Ares-Fernandez *Energy Environ. Soc.* **3** 526 (2010)
58. A Ye Yermakov, N V Mushnikov, M A Uimin, V S Gaviko, A P Tankeev, A V Skripov, A V Solonin, A L Buzlukov *J. Alloys Compd.* **425** 367 (2006)
59. O S Morozova, T I Khomenko, Ch Borchers, A V Leonov, E Z Kurmaev, A Mowes *J. Alloys Compd.* **483** 309 (2009)
60. R A Andrievski, A V Khachoyan *Ros. Khim. Zh.* **53** (2) 4 (2009) [b]
61. U Stuhr, H Wipf, T J Udovic, J Weißmüller, H Gleiter *J. Phys.: Condens. Matter* **7** 219 (1995)
62. P Kesten, A Pundt, G Schmitz, M Weisheit, H U Krebs, R Kirchheim *J. Alloys Compd.* **330 – 332** 225 (2002)
63. R Gemma, T Al-Kassab, R Kirchheim, A Pundt *Ultramicroscopy* **109** 631 (2009)
64. J Čižek, I Procházka, O S Morozova, C Borchers, A Pundt *J. Appl. Phys.* **107** 043509 (2010)
65. L Toniutti, R Checchetto, P Mengucci, A Miotello, S S Brusa *Phys. Status Solidi C* **6** 2310 (2009)
66. J Čižek, I Procházka, S Daniš, G Brauer, W Anwand, R Gemma, E Nikitin, R Kirchheim, A Pundt, R K Islamgaliev *Phys. Rev. B* **79** 054108 (2009)
67. M Krystian, D Setman, B Mingler, G Krexner, M J Zehetbauer *Scr. Mater.* **62** 49 (2010)
68. M Bönisch, M Krystian, D Setman, G Krexner, M J Zehetbauer, in *International Symposium 'Metal – Hydrogen Systems. Fundamentals and Applications' (Book of Abstracts)* Pt. I (Moscow: Moscow State University, 2010) p. 63
69. Y Fukai, N Ökuma *Phys. Rev. Lett.* **73** 1640 (1994)
70. T Iida, Y Yamazaki, T Kobayashi, Y Iijima, Y Fukai *Acta Mater.* **53** 3083 (2005)
71. Y Fukai *Defect Diff. Forum* **297 – 301** 132 (2010)
72. S Orimo, F Kimmerle, G Majer *Phys. Rev. B* **63** 094307 (2001)
73. A V Skripov, A V Soloninin, A L Buzlukov, A P Tankeyev, A E Yermakov, N V Mushnikov, M A Uimin, V S Gaviko *J. Alloys Compd.* **446 – 447** 489 (2007)
74. A V Soloninin, A V Skripov, O A Babanova, O S Morozova, A L Leonov *J. Phys. Chem. C* **114** 646 (2010)

75. R A Andrievski, A V Ragulya *Nanostrukturnye Materialy* (Nanostructural Materials) (Moscow: Akademiya, 2005)
76. S Wagner, A Pundt *Acta Mater.* **58** 1387 (2010)
77. H Akyildiz, T Öztürk *J. Alloys Compd.* **492** 745 (2010)
78. W Lohstroh, R J Westerwaal, J L M van Mechelen, H Schreuders, B Dam, R Griessen *J. Alloys Compd.* **430** 13 (2007)
79. E Kravtsov, A Nefedov, G Novak, K Zhernenkov, H Zabel, B Hjövarsson, A Liebig, A Hoser, G J McIntyre, L Paolasini, A Remhov *J. Phys.: Condens. Matter* **21** 336004 (2009)
80. M D McCluskey, S J Jokela,W M H Oo *Physica B* **376–377** 690 (2006)
81. I Jacob, S Deledda, M Bereznitsky, O Yeheskel, S M Filipek, D Mogilyanski, G Kimmel, B C Hauback, in *International Symposium 'Metal–Hydrogen Systems. Fundamentals and Applications' (Book of Abstracts)* Pt. I (Moscow: Moscow State University, 2010) p. 116
82. V Berube, G Radtke, M Dresselhaus, G Chen *Int. J. Energy Res.* **31** 637 (2007)
83. Y Levinsky *Pressure Dependent Phase Diagrams of Binary Alloys* (Materials Park, OH: ASM, 1997)
84. E Hong, D C Dunand, H Choe *Int. J. Hydr. Energy* **35** 5708 (2010)
85. M Okada, A Kamegawa, J Nakahigashi, A Yamaguchi, A Fujita, M,Yamauchi *Mater. Sci. Eng., B* **173** 253 (2010)
86. M Murzinova, G A Salishchev *Adv. Eng. Mater.* **12** 765 (2010)
87. P Chen, M Zhu *Mater. Today* **11** (12) 36 (2008)
88. I P Jain, P Jain, A Jain *J. Alloys Compd.* **503** 303 (2010)
89. K Leam, H Kazemlan, Z Yaakob, W Daud *Chem. Eng. Technol.* **33** 213 (2010)
90. A Chaise, P de Rango, Ph Marty, D Fruchart *Int. J. Hydrogen Energy* **35** 6311 (2010)
91. J Guerra, J Burt, D Ferrer, S Mejia, M Jose-Yacaman *J. Nanopart. Res.* **12** 910 (2010)
92. J Slack, J Locke, S-W Song, J Ona, Th Richardson *Sol. Energy Mater. Sol. Cells* **90** 485 (2006)
93. Th Kiefer, L Villanueva, F Fargier, F Fravier, J Brugger *Appl. Phys. Lett.* **97** 1219111 (2010)
94. M Jurczyk, L Smardz, A Szajek *Mater. Sci. Eng. B* **108** 67 (2004)
95. V I Krauz, Yu V Martynenko, N Yu Svechnikov, V P Smirnov, V G Stankevich, L N Khimchenko *Usp. Fiz. Nauk* **180** 1055 (2010) [c]
96. J Lang, J Huot *J. Alloys Compd.* **509** L18 (2011)
97. K-J Jeon, H R Moon, A M Ruminski, B Jiang, Ch Kisielowski, R Bardhan, J J Urban *Nature Mater.* **10** 286 (2011)
98. J Graetz, J Reilly, V A Yartys, J P Maehlen, B M Bulychev, V E Antonov, B P Tarasov, I E Gabis, in *International Symposium 'Metal–Hydrogen Systems. Fundamentals and Applications' (Book of Abstracts)* Pt. I (Moscow: Moscow State University, 2010) p. 5
99. A Pommerin, C Weidinthaler, F Schmth, M Felderhoff *Scr. Mater.* **62** 576 (2010)

[a] — *Chem. Sust. Develop. (Engl. Transl.)*
[b] — *Mendeleev Chem. J. (Engl. Transl.)*
[c] — *Physics-Uspekhi (Engl. Transl.)*
[d] — *Dokl. Phys. (Engl. Transl.)*
[e] — *Phys. Solid State (Engl. Transl.)*